Cell Reports
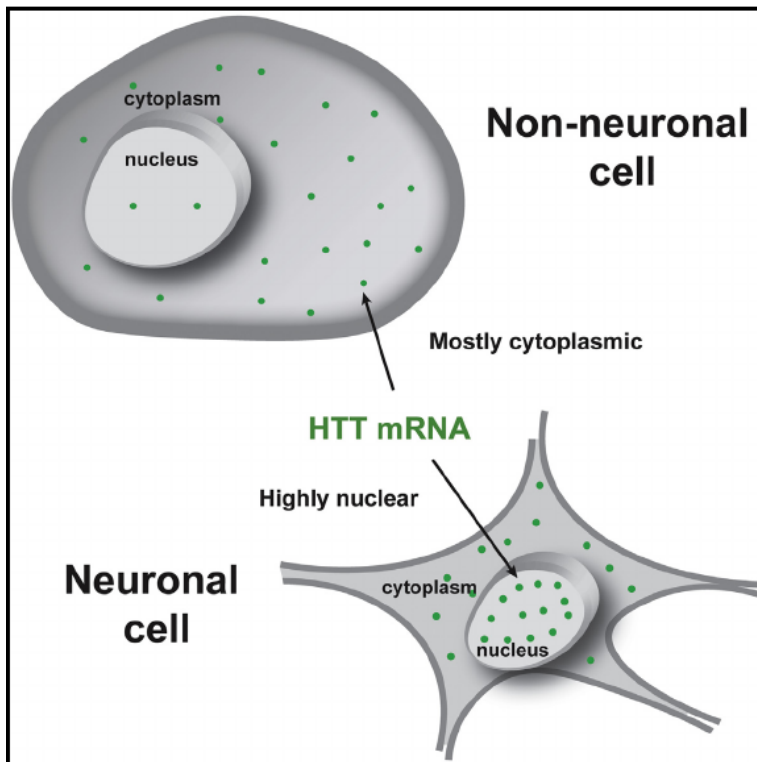
Nuclear Localization of Huntingtin mRNA Is Specific to Cells of Neuronal Origin

Graphical Abstract

Authors

Marie-Cécile Didiot, Chantal M. Ferguson, Socheata Ly, ..., Lawrence J. Hayward, Neil Aronin, Anastasia Khvorova

Correspondence

marie.didiot@umassmed.edu (M.-C.D.), anastasia.khvorova@umassmed.edu (A.K.)

In Brief

Huntington's disease (HD) is a monogenic neurodegenerative disorder representing an ideal candidate for gene silencing with oligonucleotide therapeutics. Didiot et al. examine the subcellular localization of *HTT* mRNA in non-neuronal and neuronal cells and the efficiency of oligonucleotide therapeutics on *HTT* mRNA subcellular fractions.

Highlights

- ~50% *HTT* mRNA is localized in cell nucleus

- *HTT* mRNA nuclear localization is limited to neuronal cells

- Nuclear *HTT* mRNA is more stable than cytoplasmic

- Nuclear *HTT* mRNA resists silencing by therapeutic oligonucleotides

CellPress

Report

Nuclear Localization of Huntingtin mRNA Is Specific to Cells of Neuronal Origin

Marie-Cécile Didiot,[1,*] Chantal M. Ferguson,[1] Socheata Ly,[1] Andrew H. Coles,[1] Abigail O. Smith,[1] Alicia A. Bicknell,[1,6] Lauren M. Hall,[1] Ellen Sapp,[3] Dimas Echeverria,[1] Athma A. Pai,[1] Marian DiFiglia,[3] Melissa J. Moore,[1,6] Lawrence J. Hayward,[4] Neil Aronin,[1,5] and Anastasia Khvorova[1,2,7,*]

[1]RNA Therapeutics Institute, University of Massachusetts Medical School, Worcester, MA 01605, USA
[2]Program in Molecular Medicine, University of Massachusetts Medical School, Worcester, MA 01605, USA
[3]MassGeneral Institute for Neurodegenerative Disease, Massachusetts General Hospital, Charlestown, MA 02129, USA
[4]Department of Neurology, University of Massachusetts Medical School, Worcester, MA 01605, USA
[5]Department of Medicine, University of Massachusetts Medical School, Worcester, MA 01605, USA
[6]Present address: Moderna Therapeutics, 200 Technology Square, Cambridge, MA 02139, USA
[7]Lead Contact
*Correspondence: marie.didiot@umassmed.edu (M.-C.D.), anastasia.khvorova@umassmed.edu (A.K.)
https://doi.org/10.1016/j.celrep.2018.07.106

SUMMARY

Huntington's disease (HD) is a monogenic neurodegenerative disorder representing an ideal candidate for gene silencing with oligonucleotide therapeutics (i.e., antisense oligonucleotides [ASOs] and small interfering RNAs [siRNAs]). Using an ultra-sensitive branched fluorescence *in situ* hybridization (FISH) method, we show that ~50% of wild-type *HTT* mRNA localizes to the nucleus and that its nuclear localization is observed only in neuronal cells. In mouse brain sections, we detect *Htt* mRNA predominantly in neurons, with a wide range of *Htt* foci observed per cell. We further show that siRNAs and ASOs efficiently eliminate cytoplasmic *HTT* mRNA and HTT protein, but only ASOs induce a partial but significant reduction of nuclear *HTT* mRNA. We speculate that, like other mRNAs, *HTT* mRNA subcellular localization might play a role in important neuronal regulatory mechanisms.

INTRODUCTION

Huntington's disease (HD) is an autosomal dominant neurodegenerative disorder caused by a CAG repeat expansion within exon 1 of the coding region of the *huntingtin* gene (The Huntington's Disease Collaborative Research Group, 1993). The monogenic nature of HD makes it an ideal candidate for gene silencing with oligonucleotide therapeutics, such as antisense oligonucleotides (ASOs) and short interfering RNAs (siRNAs), which are both involved in post-transcriptional gene silencing by reducing the target mRNA levels (for review, Crooke et al., 2018). siRNAs induce mRNA degradation by loading into the RNA-induced silencing complex (RISC) in the cytoplasm, and ASOs promote mRNA degradation via RNase H in both the nucleus and the cytoplasm.

In the central dogma of cellular biology, the mRNAs are predominantly localized in the cytoplasm in mammalian cells.

Therefore, both classes of therapeutics are highly efficient at silencing mRNA expression, presumably due to the cytoplasmic localization of mRNA. When studying *HTT* mRNA silencing in different cell types, we observed that siRNA treatment fully silenced *HTT* in HeLa cells (>95%) but only reduced *Htt* by 50%–70% in mouse primary neurons (Alterman et al., 2015). To understand the reason(s) behind this discrepancy in the degree of silencing in different cell types, we wanted to carefully visualize the cellular distribution of *Htt* mRNA in individual cells. We hypothesized that the differences in silencing efficacy were due to a difference in cellular localization of *Htt* mRNA between cell types.

In this study, we used a highly sensitive, branched fluorescence *in situ* hybridization (FISH) technology—RNAscope (Wang et al., 2012)—and confocal microscopy to observe and quantify the intracellular distribution of *HTT* mRNA at high resolution in single cells. We found that a significant fraction of *HTT* mRNA localizes to the nucleus of neuronal cells, but not non-neuronal cells. This cellular localization of *HTT* mRNA affects its silencing by therapeutic oligonucleotides both *in vitro* and *in vivo*: siRNAs and ASOs nearly eliminated cytoplasmic *HTT* mRNA and only ASOs partially reduced nuclear *HTT* mRNA levels. Our findings reveal a new parameter for consideration in our understanding of the role of HTT mRNA in neuronal regulatory mechanisms and oligonucleotide therapeutic development.

RESULTS

Branched FISH Technology Enables Precise *In Situ* Detection of Spliced *Htt* mRNA

Previously, CAG-specific probes have been used as a proxy for *HTT* mRNA detection (de Mezer et al., 2011; Urbanek et al., 2017). However, we observed intense CAG FISH staining throughout the nucleus and cytoplasm, and a very low fraction of the CAG-FISH signal co-localized with the FISH signal using an *HTT* mRNA-specific probe set (Figures S1A and S1B). Thus, we implemented and validated a highly sensitive and specific branched FISH technology to detect *Htt* mRNA.

To ensure the specific detection of *Htt* mRNA by the FISH assay, we developed a panel of probes that target different

regions of *Htt* mRNA and independent targets and used the following controls (Table S1; Figure S1): (1) co-targeting of *Htt* mRNA and CAG repeat (Figures S1A–S1D); (2) co-targeting the same *Htt* mRNA region (exons 27–35 [E27–35]) in two different fluorescent channels (488 and 570 nm; Figures S1E–S1H); (3) co-targeting of two different regions of *Htt* mRNA (E1–7 and E27–35; Figures S1I–S1L); (4) co-targeting exonic (E27–35) and intronic (I61) regions of *Htt* mRNA (Figures S1M and S1N); and (5) co-targeting *Htt* mRNA and *Herc2* mRNA (Figures S1O and S1P). To accurately estimate the number of mRNA foci per cell and ensure that intracellular distribution (nucleus versus cytoplasm) does not affect mRNA quantification, we quantified mRNA foci in three dimensions throughout the volume of each cell (see STAR Methods for details).

We observed up to 70% and 80% of FISH foci co-localization using probe sets that target similar or different regions of the *Htt* mRNA (Figures S1F and S1J) and no co-localization of *Htt* mRNA foci with *Herc2* mRNA foci (Figure S1P). Background co-localization (calculated by rotating one channel 180°) did not exceed 1% in most samples (Figures S1G, S1H, S1K, and S1L). The exception was the CAG-specific probe set, which resulted in ~10% background co-localization, which is expected for probes that stain hundreds of foci per cell (Figures S1C and S1D). In addition, we observed that the majority of nuclear *Htt* mRNA foci localized in the nucleus appeared to be spliced (Figures S1M and S1N).

More Than 50% of *Htt* mRNA Is Localized to the Nucleus in Mouse Primary Neurons

We assessed the intracellular distribution of *Htt* and control mRNAs in mouse primary cortical neurons (Figures S2A–S2E). Precise quantification of mRNA foci by FISH showed ~200 *ActB*, ~25 *Ppib*, ~30 *Hprt*, ~37 *Herc2*, and ~20 *Htt* foci per cell (Figures S2A and S2B). Whereas most housekeeping mRNAs localized primarily in the cytoplasm (90% *Ppib*, ~80% *ActB*, and ~80% *Hprt*), 60% of *Htt* mRNA localized in the nucleus. The nuclear enrichment of *Htt* mRNA was not an artifact of mRNA length; we observed only 40% nuclear localization of *Herc2* mRNA, which is longer than *Htt* mRNA (Table S1). As expected, the long non-coding RNAs (lncRNAs) *Neat1* and *Malat1* were only detected in the nucleus (Figures S2A and S2C). To confirm *Htt* mRNA localization patterns observed by FISH and ensure that the probe hybridization is similar in nucleus and cytoplasm, we performed RT-qPCR to quantify nuclear and cytoplasmic *ActB*, *Herc2*, and *Htt* mRNA fractions isolated from primary neurons. The data showed that *Htt* mRNA is significantly more enriched in the nuclear fraction than *ActB* or *Herc2* mRNA (respectively, ***p < 0.001 and *p < 0.05; Figures S2D and S2E). Thus, *Htt* mRNA shows an unusual enrichment in the nuclei of mouse primary neurons.

To determine whether the non-dividing characteristic of neurons affects *Htt* mRNA subcellular localization, we assessed mRNA distribution in dividing cells of neuronal origin (Neuro2a cells; Figure S2F). Precise transcript quantification showed an average of ~30 *Htt*, ~115 *Ppib*, ~75 *Hprt*, and ~27 *Herc2* mRNA foci per cell (Figure S2G). Whereas the control *Hprt*,

Ppib, and *Herc2* mRNA foci were all predominantly cytoplasmic (90%, 71%, and 64%), most *Htt* mRNA foci were nuclear (68%). As expected, almost all *Neat1* lncRNA foci were nuclear (95%; Figures S2G and S2H). Thus, nuclear enrichment of *Htt* mRNA is observed in both dividing and non-dividing cells of neuronal origin.

Htt mRNA Nuclear Localization Is Specific to Cells of Neuronal Origin

To determine the effect of cell type on *Htt* mRNA localization, we compared *Htt* mRNA distribution in non-neuronal cells (i.e., HeLa, human primary fibroblasts, and mouse primary fibroblasts) to that observed in cells of neuronal origin (i.e., mouse Neuro2a cells, cortical primary neurons, and mouse brain tissue). Whereas ~50% of *Htt* mRNA foci localized to the nucleus in neuronal cells, only 10%–20% of *Htt* mRNA foci were nuclear in non-neuronal cells (Figures 1A–1C). These findings agree with our observation that siRNA can completely silence *Htt* mRNA in HeLa cells, but not in primary neurons.

In both primary neurons and brain sections, we observed significant cell-to-cell variability in both *Htt* mRNA expression and subcellular localization. To evaluate *Htt* mRNA level and distinguish between neuronal and non-neuronal cells in the brain, we developed and optimized a dual FISH-immunofluorescence approach that allows simultaneous detection of mRNA and protein. NeuN and GFAP were, respectively, used as markers for neurons (Figure 2) and glial cells (Figure S3). *Htt* mRNA in the brain was almost entirely neuronal. Moreover, the number of *Htt* mRNA foci varied widely between neurons: undetectable in some neurons and as many as 60 foci in others (Figures 2A, 2B, S3A, and S3B). On average, we observed ~17 *Htt* mRNA foci per cell, with ~55% of foci in the nucleus (Figures 2B, 2D, S3C, and S3D). These data quantitatively confirm the previous findings that *Htt* mRNA is predominantly expressed in neurons *in vivo* (http://proteinatlas.org).

Human Fibroblast Reprogramming into Neuron-like Cells Changes *HTT* mRNA Nuclear-Cytoplasmic Distribution

Human adult fibroblasts, which express cytoplasmic *Htt* mRNA, can be reprogrammed directly into neuron-like cells by overexpressing miR-9 and miR-124 and several neuronal transcription factors (Richner et al., 2015; Tang et al., 2013). We therefore tested whether trans-differentiation of fibroblasts into neuron-like cells affects *HTT* mRNA subcellular distribution (Figure 3). Upon the induction of miR-9 and miR-124 expression (Figure 3A), cells gradually acquired a neuronal morphology characterized by reduction of the cytoplasm and the development of neuronal projections (Figure 3B). Before trans-differentiation, ~90% of *HTT* mRNA foci were cytoplasmic. In trans-differentiated neuron-like cells, ~60% of *HTT* mRNA foci were nuclear (Figures 3C–3E). The change in the nuclear-cytoplasmic ratio is accompanied by a sharp decrease in the number of cytoplasmic foci, suggesting that the rate of nucleo-cytoplasmic export of *Htt* mRNA might differ in neuronal and non-neuronal cells. Thus,
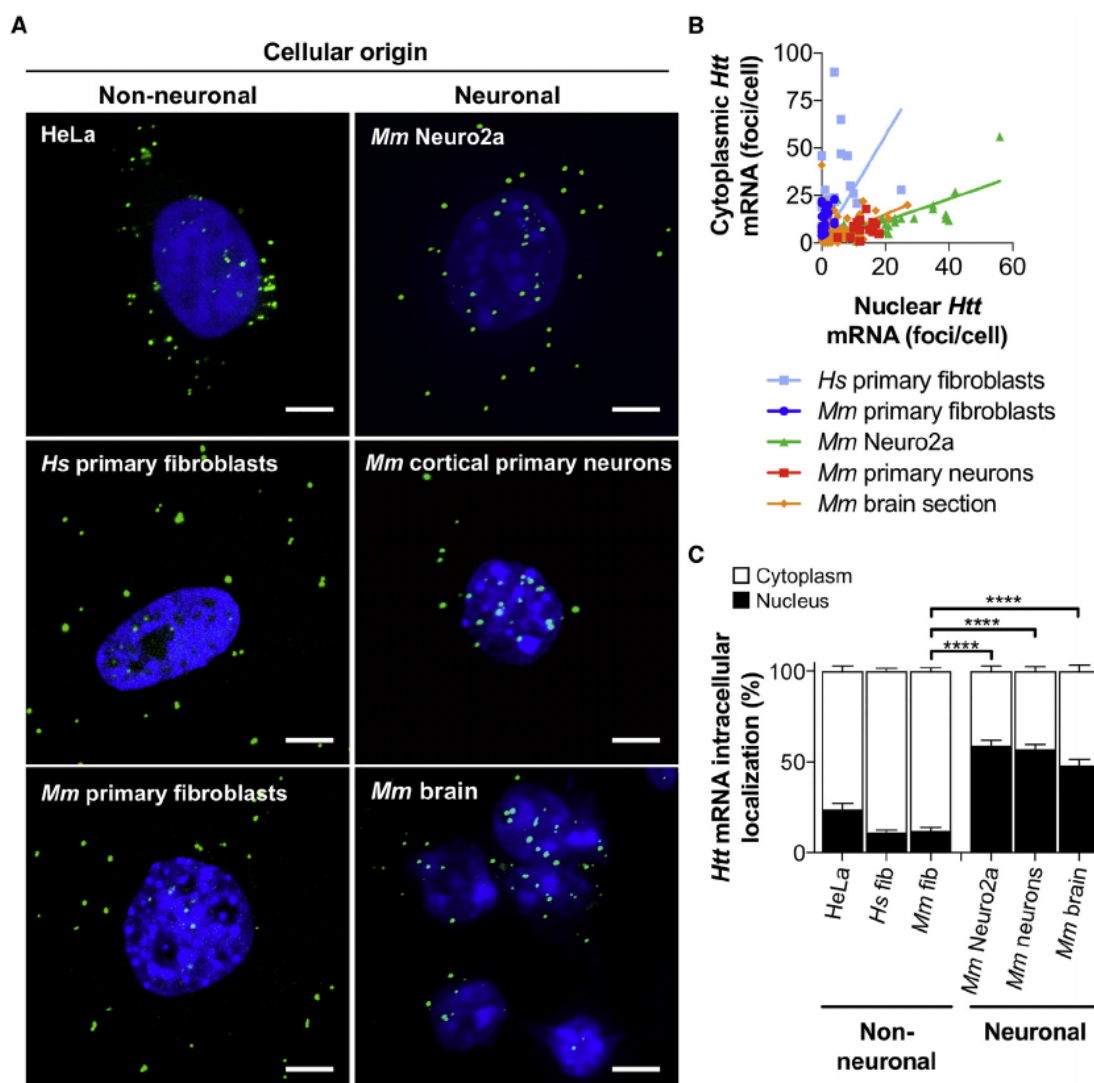
Figure 1. *Htt* mRNA Is Highly Retained in the Nucleus in Cells of Neuronal Origin

(A) *Htt* mRNA (green) detected in cells of non-neuronal origin (HeLa, *Hm*, and *Mm* primary fibroblasts) and in cells of neuronal origin (*Mm* Neuro2a, *Mm* cortical primary neurons, and *Mm* brain section) by dual-color FISH. Nuclei are labeled with Hoechst (blue). Representative images of maximum Z projections of optical sections through the nucleus are spaced 0.5 μm apart. 100× oil objective is shown (scale bars, 5 μm).

(B) Scatterplot representing the absolute quantification of *Htt* transcript in each cell line. Each dot represents the number of nuclear and cytoplasmic foci for one cell (n = 20–30 cells). Linear regression is shown for each transcript.

(C) Percentage of nuclear and cytoplasmic localization of *Htt* mRNA in different cell lines (n ∼20 cells; mean ± SEM; ****p < 0.0001; one-way ANOVA-Bonferroni's multiple comparisons test).

See also Figure S2.

cell type, rather than origin, is crucial in defining *HTT mRNA* cellular localization.

Nuclear *Htt* mRNA Is More Stable than Cytoplasmic *Htt* mRNA

Several cellular processes might contribute to nuclear retention of *Htt* mRNA in neuronal cells, including slow nuclear-cytoplasmic export or rapid cytoplasmic mRNA turnover. To determine the rate of *Htt* mRNA turnover, we blocked RNA polymerase II (Pol II)-mediated transcription and quantified mRNA levels at 2, 4, 6, 8, and 10 hr post-transcriptional inhibition (Figures S4A–S4C). Cytoplasmic *Htt* mRNA levels (4-hr half-life) decreased significantly faster than nuclear *Htt* mRNA (10-hr half-life; ****p < 0.0001; Figures S4A and S4B). By contrast, *Herc2* mRNA turned over at the same rate in both nuclear and cytoplasmic fractions (∼6-hr half-life; Figure S4C). The cytoplasmic *Htt* and *Herc2* mRNAs decreased at similar rates, and nuclear *Htt* mRNA decreased at a significantly slower rate than *Herc2* mRNA (Figures S4B and S4C).
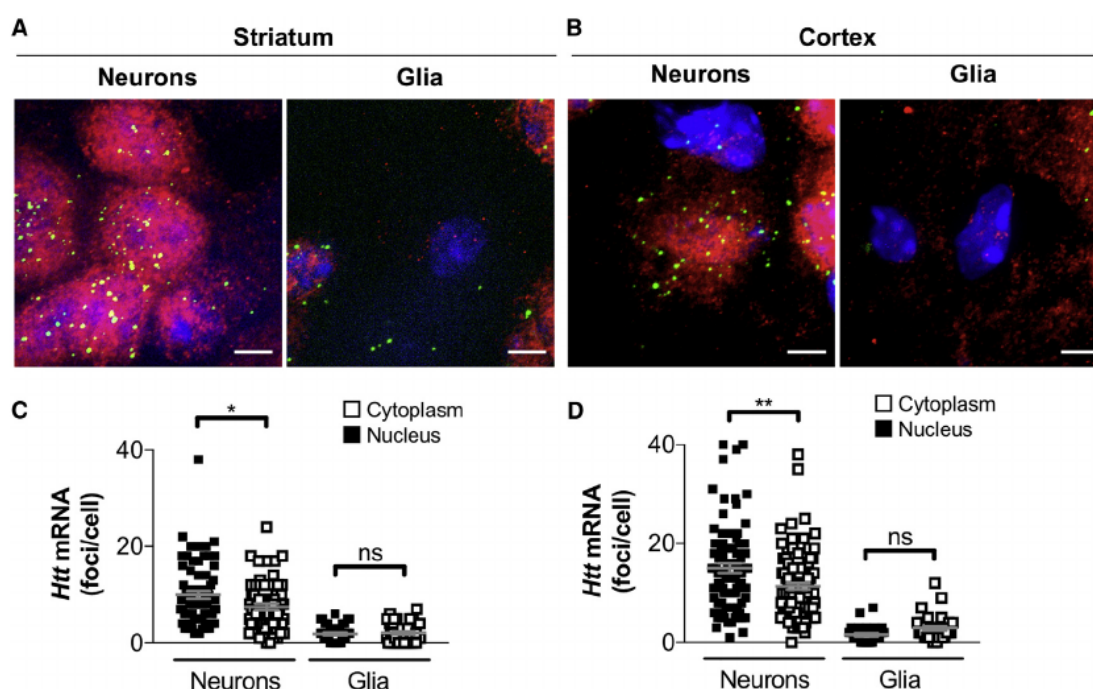
Figure 2. A Large Fraction of *Htt* mRNA Is Localized in the Nucleus of Striatal and Cortical Neurons in Mouse Brain
(A and B) *Htt* mRNA (green) detected in neurons (NeuN-positive cells, red) and glia (NeuN-negative cells) in the (A) striatum and the (B) cortex. Nuclei labeled with Hoechst (blue) are shown. Representative images are maximum Z projections of >20 optical sections spaced 0.5 μm apart. 100× oil objective for neuronal type cells is shown (scale bars, 5 μm).
(C and D) Scatter graph of nuclear and cytoplasmic *Htt* mRNA foci in (C) the striatum and (D) the cortex (n = 20–30 cells; mean ± SEM; *p < 0.05; **p < 0.01; one-way ANOVA-Bonferroni's multiple comparisons test).
See also Figure S3.

Nuclear *Htt* mRNA Resists Silencing by Both ASOs and siRNAs

Our findings suggest that the neuronal-specific nuclear enrichment of *Htt* mRNA could explain why siRNAs cannot fully silence *Htt* mRNA in neuronal cells. We therefore directly tested whether the subcellular localization of *Htt* mRNA affects its ability to be silenced by therapeutic oligonucleotides (Figures 4 and S4E–S4K).

Mouse primary neurons were treated for 7 days with either LNA GapmeR ASO targeting position 3,209 in *Htt* exon 23 (ASO[HTT]) (Hung and Leeds, 2007) or chemically stabilized, hydrophobic siRNA targeting position 10,150 in *Htt* 3′ UTR (siRNA[HTT]) (Alterman et al., 2015). Sequence and chemical composition of compounds used are shown in Table S2. FISH analysis of treated neurons showed that both chol-siRNA[HTT] and DHA-siRNA[HTT] reduced cytoplasmic *Htt* mRNA foci by 90% (Figures S4E and S4H), but not nuclear *Htt* mRNA foci. ASO[HTT] significantly reduced the number of cytoplasmic and nuclear *Htt* foci (by 80% and 40%; Figure S4E). There was no major impact of both siRNAs and ASOs on *Hprt* and *Herc2* mRNA foci level and localization (Figures S4F and S4G). siRNA and ASO cytotoxicity, measured using the alamar blue assay, showed that the primary neurons' viability was not altered by the treatment at the indicated concentrations (Figure S4H). To evaluate siRNAs' and ASOs' silencing efficiency, we measured the total cellular level of *Htt* mRNA using the QuantiGene assay. We observed 60% *Htt*

mRNA silencing in cells treated with 0.15 μM ASO[HTT] or siRNA[HTT] (Figure S4K), consistent with previous observations. At 1.25 μM concentration, ASO[HTT] reduced total *Htt* mRNA by ~85%, whereas siRNA[HTT] only reduced total *Htt* mRNA by ~75%, consistent with the possibility that siRNAs mostly silence cytoplasmic *Htt* mRNA and ASOs silence both nuclear and cytoplasmic *Htt* mRNA. Consistent with efficient silencing of cytoplasmic *Htt* mRNA, both therapeutic oligonucleotides significantly reduced HTT protein levels (Figures S4I and S4J).

We evaluated the impact of *Htt* mRNA subcellular distribution on oligonucleotide efficiency *in vivo* (Figure 4). When injected directly in mouse striatum, DHA-siRNAs induced efficient *Htt* mRNA silencing and had no measurable impact on neuronal integrity or innate immune activation (Nikan et al., 2016). Mice were directly injected with 4 nmol DHA-siRNA[NTC], DHA-siRNA[HTT] (Nikan et al., 2016), ASO[NTC], and ASO[HTT] (Hung and Leeds, 2007) in the right striatum (n = 3 animals per group; Figure 4A). After 7 days, levels of nuclear and cytoplasmic *Htt* mRNA foci were assessed by FISH (Figures 4B and 4C). Consistent with the data obtained *in vitro*, we observed that DHA-siRNA[HTT] reduced cytoplasmic *Htt* mRNA foci by 95%, but not nuclear *Htt* mRNA foci. In contrast, ASO[HTT] significantly reduced the number of both cytoplasmic and nuclear *Htt* foci by 90% and 60%, respectively (Figure 4D). We did not detect any significant impact by either siRNA or ASO on *Hprt* and *Herc2* mRNA foci level and localization (Figures 4E and 4F).
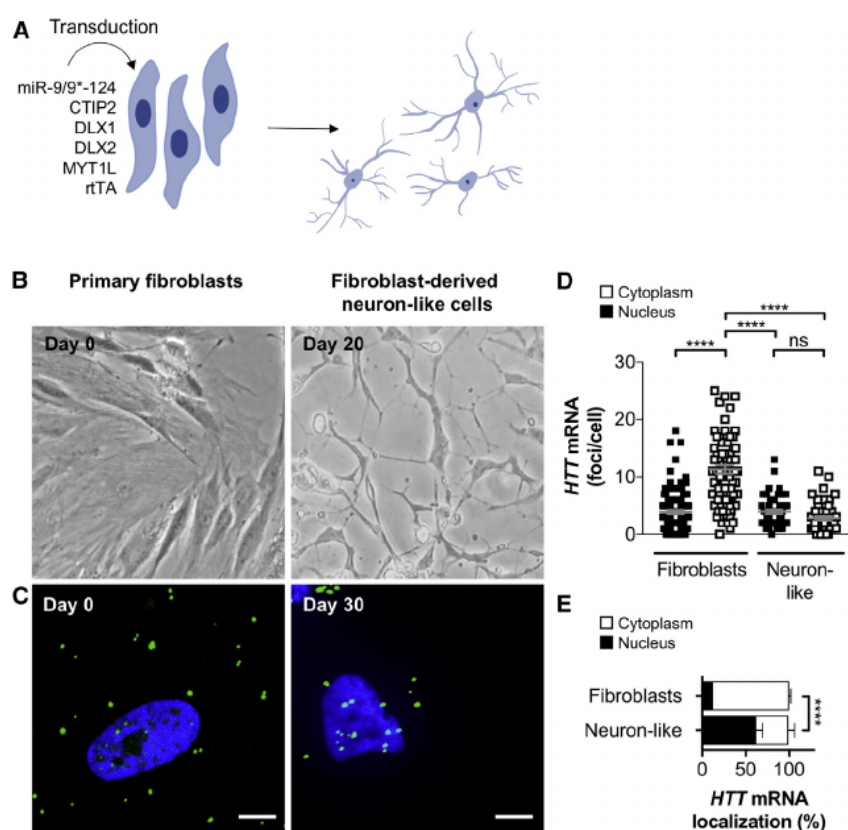
Figure 3. A Large Fraction of *Htt* mRNA Is Localized in the Nucleus of Fibroblast-Derived Neuron-like Cells

(A) Scheme of fibroblasts conversion to neurons showing the neuronal morphology acquisition (adapted from Richner et al., 2015).

(B) Phase contrast images of human primary fibroblasts transduced with miR-9/9*-124 and CDM at post-induction dates (PIDs) 20.

(C) *Htt* mRNA (green) was detected by FISH in *Hs* primary fibroblasts and *Hs* primary fibroblast-derived neuron-like cells. Nuclei labeled with Hoechst (blue) are shown. Representative images are maximum Z projections of >20 optical sections spaced 0.5 μm apart. 100× oil objective for neuronal type cells is shown (scale bars, 5 μm).

(D) Scatterplot of nuclear and cytoplasmic *Htt* mRNA foci (n = 20–30 cells; mean ± SEM; ns, not significant; ****p < 0.0001; one-way ANOVA-Bonferroni's multiple comparisons test).

(E) Percentage of nuclear and cytoplasmic localization for *Htt* transcript (n = 20–30 cells; mean ± SEM; ****p < 0.0001; one-way ANOVA-Bonferroni's multiple comparisons test).

DISCUSSION

The HD gene *Htt* is expressed throughout the body, but HD pathology is primarily limited to neuronal tissues. Using branched FISH, high-resolution confocal microscopy, and volumetric quantification of mRNA foci, we show that wild-type *Htt* mRNAs (with a normal number of CAG repeats) accumulate in the nucleus of neuronal cells, but not in non-neuronal cells. A similar *Htt* distribution pattern was demonstrated by the analysis of RNA sequencing (RNA-seq) datasets from human embryonic stem cell (HESC)-derived neurons (Blair et al., 2017; Figure S3E). The results showed that, relative to the total number of reads in each sample, *Htt* transcript is detected more often in the nuclear fraction than in the cytoplasmic fraction. These findings suggest that *Htt* mRNA processing, export, or stability is differentially regulated in neuronal cells both *in vitro* and *in vivo*.

Advances in oligonucleotide therapeutics have put effective treatments for HD within reach (Kordasiewicz et al., 2012; http://www.ionispharma.com). Therapeutic oligonucleotides cause gene silencing by directing mRNA destruction, thereby preventing the expression of proteins involved in genetic disease. Whereas ASOs target mRNAs in the nucleus and cytoplasm, siRNAs primarily target mRNAs in the cytoplasm (this study and Castanotto et al., 2015). We have found that ASOs partially but significantly reduce the nuclear fraction of *Htt*, and siRNAs do not silence nuclear *Htt* mRNA at the used concentrations used. Regardless of the oligonucleotide used, nuclear *Htt* mRNA is more resistant to silencing than cytoplasmic *Htt* mRNA. The resistance of nuclear *Htt* mRNA to silencing by oligonucleotides could be related to the increased stability or retention of nuclear *Htt* mRNA compared to cytoplasmic *Htt* mRNA. Future studies are needed to understand the compartment efficiency of various oligonucleotides on wild-type and mutant *Htt* and for the development and optimization of therapeutics to treat HD and other neurodegenerative diseases.

The investigation of *Htt* mRNA distribution in brain sections revealed a high degree of variability in levels of *Htt* mRNA expression between different cell types (neurons versus glia) and within the same cell types. In general, neurons express significantly more *Htt* mRNA than glia. Similarly, detection of *HTT* mRNA in wild-type human brain by immunohistochemistry showed higher level of *HTT* mRNA in neurons than in glia (Landwehrmeyer et al., 1995). These data are consistent with data from RNA-seq datasets performed on various cell population of mouse cerebral cortex and suggest *Htt* mRNA is predominantly expressed in neurons compared to glia (Zhang et al., 2014; Figure S3F).
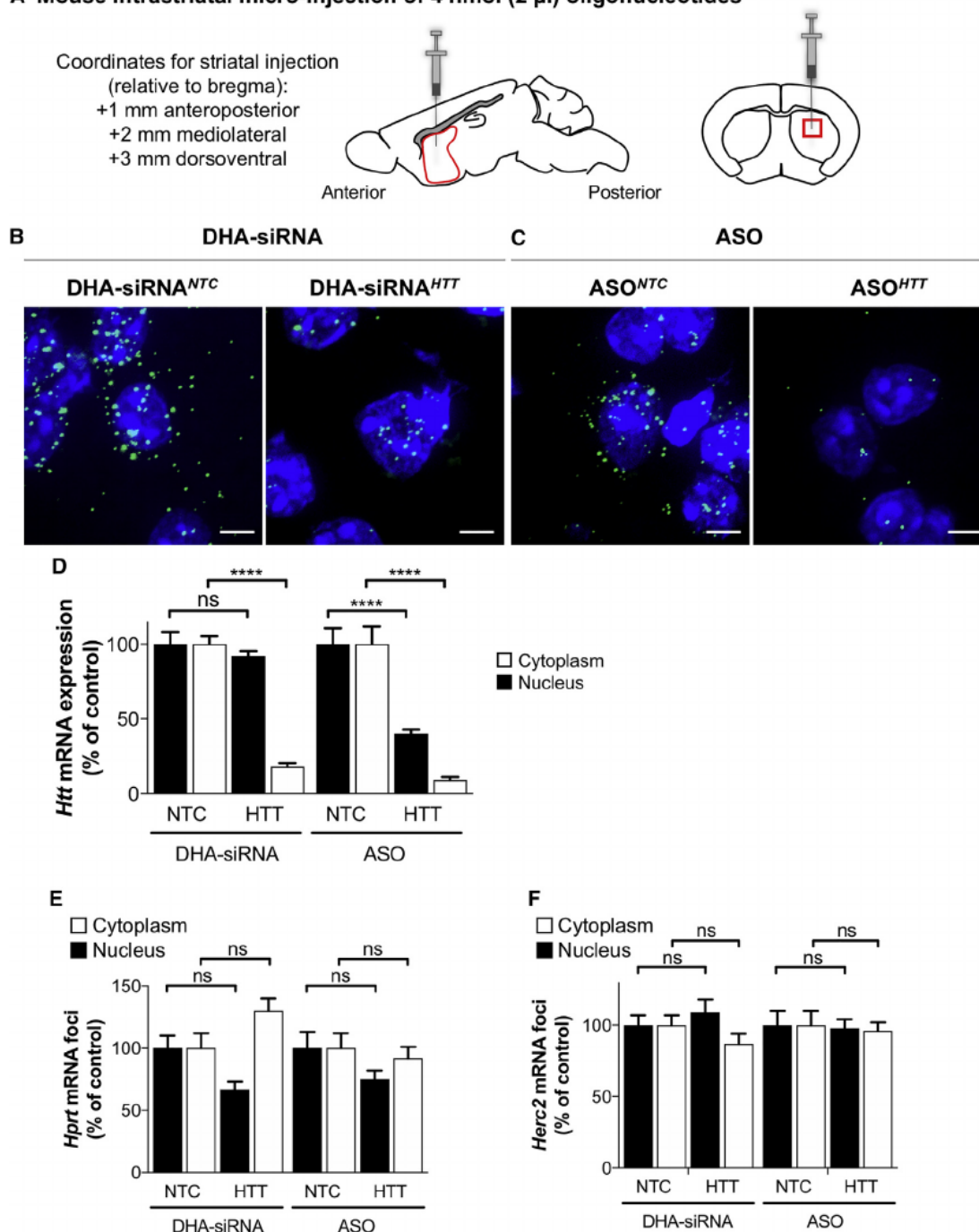
Interestingly, as previously described, we also observed a substantial variability of *Htt* mRNA level between individual neurons, with neurons not expressing *Htt* mRNA and neurons expressing as many as 60 copies per cell (Keeler et al., 2016). Several studies have demonstrated that the cell to cell variability is a biological phenomenon and could play critical roles in determining biologically and clinically significant phenotypes (for review, Patange et al., 2018). *HTT* mRNA subcellular distribution, as well as expression variability, may provide valuable information about HTT function in neuronal regulatory mechanisms.

Figure 4. *In Vivo Htt* mRNA Silencing in Striatal Neurons by Hydrophobically Modified siRNA and Antisense Oligonucleotides

DHA-siRNA[NTC], DHA-siRNA[HTT], ASO[NTC], and ASO[HTT] (4 nmol in 2 μL; n = 3 animals per group) were administered by unilateral intrastriatal bolus microinjection. Brains were collected after 7 days, and *Htt* mRNA foci subcellular levels were assessed by FISH.

(A) Schematic diagram of sagittal and coronal sections through the mouse striatum at the site of injection. The striatal region selected to acquire the images (red box) is indicated.

(B and C) FISH detection of *Htt* mRNA (green) upon (B) DHA-siRNA and (C) ASO treatments. Nuclei labeled with Hoechst (blue) are shown. Representative images are maximum Z projections through the nuclear region spaced 0.5 μm apart. 100× oil objective is shown (scale bars, 5 μm).

Summary and Conclusion

Using branched FISH, we localize and quantify wild-type *Htt* mRNA (non-expanded CAG repeat) in different cell types and evaluate the differential silencing efficiency of ASOs and siRNAs on nuclear versus cytoplasmic *Htt* mRNA. We show that more *Htt* mRNA is nuclear in neuronal cells compared to non-neuronal cells. Furthermore, we show that siRNAs and ASOs differentially silence nuclear and cytoplasmic *Htt* mRNA. This is the first detailed observation of a clear change in *Htt* mRNA intracellular localization based on cellular identity and the first investigation of the differential subcellular efficacy of different oligonucleotide therapies. These results provide insight into the characteristics of *Htt* mRNA, incite future investigation into the subcellular distribution of mutant *Htt* mRNA, and identify a new aspect for consideration in the development of future oligonucleotide therapeutics targeting *HTT* mRNA.

STAR METHODS

Detailed methods are provided in the online version of this paper and include the following:

SUPPLEMENTAL INFORMATION

Supplemental Information includes four figures and two tables and can be found with this article online at https://doi.org/10.1016/j.celrep.2018.07.106.

AUTHOR CONTRIBUTIONS

Conceptualization, M.-C.D., A.K., and N.A.; Investigation, M.-C.D., C.M.F., A.H.C., A.O.S., A.A.B., L.M.H., and E.S.; siRNAs Synthesis and QC, D.E.; Formal Analysis, M.-C.D., C.M.F., S.L., A.A.P., and A.K.; Software (ImageJ Macro), S.L. and L.J.H.; Results and Discussion, M.-C.D., C.M.F., M.J.M., N.A., and A.K.; Writing, M.-C.D., C.M.F., N.A., and A.K.

DECLARATION OF INTERESTS

The authors declare no competing interests.

REFERENCES

Alterman, J.F., Hall, L.M., Coles, A.H., Hassler, M.R., Didiot, M.C., Chase, K., Abraham, J., Sottosanti, E., Johnson, E., Sapp, E., et al. (2015). Hydrophobically modified siRNAs silence Huntingtin mRNA in primary neurons and mouse brain. Mol. Ther. Nucleic Acids *4*, e266.

Alterman, J.F., Coles, A.H., Hall, L.M., Aronin, N., Khvorova, A., and Didiot, M.C. (2017). A high-throughput assay for mRNA silencing in primary cortical neurons in vitro with oligonucleotide therapeutics. Biol. Protoc. *7*, e2501.

Blair, J.D., Hockemeyer, D., Doudna, J.A., Bateup, H.S., and Floor, S.N. (2017). Widespread translational remodeling during human neuronal differentiation. Cell Rep. *21*, 2005–2016.

Bolte, S., and Cordelières, F.P. (2006). A guided tour into subcellular colocalization analysis in light microscopy. J. Microsc. *224*, 213–232.

Castanotto, D., Lin, M., Kowolik, C., Wang, L., Ren, X.Q., Soifer, H.S., Koch, T., Hansen, B.R., Oerum, H., Armstrong, B., et al. (2015). A cytoplasmic pathway for gapmer antisense oligonucleotide-mediated gene silencing in mammalian cells. Nucleic Acids Res. *43*, 9350–9361.

Crooke, S.T., Witztum, J.L., Bennett, C.F., and Baker, B.F. (2018). RNA-targeted therapeutics. Cell Metab. *27*, 714–739.

de Mezer, M., Wojciechowska, M., Napierala, M., Sobczak, K., and Krzyzosiak, W.J. (2011). Mutant CAG repeats of Huntingtin transcript fold into hairpins, form nuclear foci and are targets for RNA interference. Nucleic Acids Res. *39*, 3852–3863.

Hung, G., and Leeds, J. (2007). Compositions and their uses directed to huntingtin. US patent application publication 20150307877 A1, filed January 5, 2015, and published October 29, 2015.

Keeler, A.M., Sapp, E., Chase, K., Sottosanti, E., Danielson, E., Pfister, E., Stoica, L., DiFiglia, M., Aronin, N., and Sena-Esteves, M. (2016). Cellular analysis of silencing the Huntington's disease gene using AAV9 mediated delivery of artificial micro RNA into the striatum of Q140/Q140 mice. J. Huntingtons Dis. *5*, 239–248.

(D–F) Quantification of (D) *Htt*, (E) *Hprt*, and (F) *Herc2* mRNA foci number. mRNA foci levels are presented as percentage of non-targeting control (n > 100 cells from 3 biological replicates; mean ± SEM; ****p < 0.0001; one-way ANOVA-Bonferroni's multiple comparisons test). ASO, antisense oligonucleotide; DHA-siRNA, docosahexaenoic acid-siRNA conjugate; NTC, non-targeting control; siRNA, small interfering RNA.
See also Figure S4 and Table S2.

Kordasiewicz, H.B., Stanek, L.M., Wancewicz, E.V., Mazur, C., McAlonis, M.M., Pytel, K.A., Artates, J.W., Weiss, A., Cheng, S.H., Shihabuddin, L.S., et al. (2012). Sustained therapeutic reversal of Huntington's disease by transient repression of huntingtin synthesis. Neuron 74, 1031–1044.

Landwehrmeyer, G.B., McNeil, S.M., Dure, L.S., 4th, Ge, P., Aizawa, H., Huang, Q., Ambrose, C.M., Duyao, M.P., Bird, E.D., Bonilla, E., et al. (1995). Huntington's disease gene: regional and cellular expression in brain of normal and affected individuals. Ann. Neurol. 37, 218–230.

Nikan, M., Osborn, M.F., Coles, A.H., Godinho, B.M., Hall, L.M., Haraszti, R.A., Hassler, M.R., Echeverria, D., Aronin, N., and Khvorova, A. (2016). Docosahexaenoic acid conjugation enhances distribution and safety of siRNA upon local administration in mouse brain. Mol. Ther. Nucleic Acids 5, e344.

Ollion, J., Cochennec, J., Loll, F., Escudé, C., and Boudier, T. (2013). TANGO: a generic tool for high-throughput 3D image analysis for studying nuclear organization. Bioinformatics 29, 1840–1841.

Otsu, N. (1979). A threshold selection method from gray-level histograms. IEEE Trans. Syst. Man Cybern. 9, 62–66.

Patange, S., Girvan, M., and Larson, D.R. (2018). Single-cell systems biology: probing the basic unit of information flow. Curr. Opin. Syst. Biol. 8, 7–15.

Richner, M., Victor, M.B., Liu, Y., Abernathy, D., and Yoo, A.S. (2015). MicroRNA-based conversion of human fibroblasts into striatal medium spiny neurons. Nat. Protoc. 10, 1543–1555.

Sapp, E., Valencia, A., Li, X., Aronin, N., Kegel, K.B., Vonsattel, J.P., Young, A.B., Wexler, N., and DiFiglia, M. (2012). Native mutant huntingtin in human brain: evidence for prevalence of full-length monomer. J. Biol. Chem. 287, 13487–13499.

Schneider, C.A., Rasband, W.S., and Eliceiri, K.W. (2012). NIH Image to ImageJ: 25 years of image analysis. Nat. Methods 9, 671–675.

Seluanov, A., Vaidya, A., and Gorbunova, V. (2010). Establishing primary adult fibroblast cultures from rodents. J. Vis. Exp., 2033.

Tang, J., Yoo, A.S., and Crabtree, G.R. (2013). Reprogramming human fibroblasts to neurons by recapitulating an essential microRNA-chromatin switch. Curr. Opin. Genet. Dev. 23, 591–598.

The Huntington's Disease Collaborative Research Group (1993). A novel gene containing a trinucleotide repeat that is expanded and unstable on Huntington's disease chromosomes. Cell 72, 971–983.

Urbanek, M.O., Fiszer, A., and Krzyzosiak, W.J. (2017). Reduction of Huntington's disease RNA foci by CAG repeat-targeting reagents. Front. Cell. Neurosci. 11, 82.

Wang, F., Flanagan, J., Su, N., Wang, L.C., Bui, S., Nielson, A., Wu, X., Vo, H.T., Ma, X.J., and Luo, Y. (2012). RNAscope: a novel in situ RNA analysis platform for formalin-fixed, paraffin-embedded tissues. J. Mol. Diagn. 14, 22–29.

Zack, G.W., Rogers, W.E., and Latt, S.A. (1977). Automatic measurement of sister chromatid exchange frequency. J. Histochem. Cytochem. 25, 741–753.

Zhang, Y., Chen, K., Sloan, S.A., Bennett, M.L., Scholze, A.R., O'Keeffe, S., Phatnani, H.P., Guarnieri, P., Caneda, C., Ruderisch, N., et al. (2014). An RNA-sequencing transcriptome and splicing database of glia, neurons, and vascular cells of the cerebral cortex. J. Neurosci. 34, 11929–11947.

STAR METHODS

KEY RESOURCES TABLE

REAGENT or RESOURCE	SOURCE	IDENTIFIER
Antibodies		
rabbit polyclonal anti-HTT	Sapp et al., 2012	Ab1; RRID: N/A
rabbit polyclonal anti-RPB1	Cell Signaling	Cat#2629; RRID: AB_2167468
mouse monoclonal anti-GAPDH	Sigma	Cat#MAB374; RRID: AB_2107445
chicken monoclonal anti-NeuN	Millipore	Cat#MAB377B; RRID: AB_177621
chicken polyclonal anti-GFAP	Millipore	Cat#AB5541; RRID: AB_177521
Chemicals, Peptides, and Recombinant Proteins		
AlamarBlue	Life Technologies	Cat#DAL1025
Critical Commercial Assays		
See Table S1 for the list and cat# of RNAscope probes	ACDBio	N/A
RNAscope Fluorescent Multiplex Assay	ACDBio	Cat#320850
QuantiGene 2.0 Assay	Affymetrix	Cat#QS0011
QuantiGene 2.0 *Htt* probe	Affymetrix	Cat#SB-14150
QuantiGene 2.0 *Ppib* probe	Affymetrix	Cat#SB-10002
Experimental Models: Cell Lines		
Mouse: Neuro2a	ATCC	Cat#CCL-131
Mouse: embryonic day 16 cortical primary neurons	N/A	N/A
Mouse: primary fibroblasts	N/A	N/A
Human: HeLa	ATCC	Cat#CCL-2
Human: primary fibroblasts	Coriell	Cat#GM08399
Experimental Models: Organisms/Strains		
Mouse: wild-type FVB/NJ (female)	The Jackson Laboratory	Cat#001800
Oligonucleotides		
Chol-siRNA^{HTT}	Alterman et al., 2015	hsiRNA HTT10150
Chol-siRNA^{NTC}	Alterman et al., 2015	hsiRNA NTC
DHA-siRNA^{HTT}	Nikan et al., 2016	DHA-hsiRNA^{HTT}
DHA-siRNA^{NTC}	Nikan et al., 2016	DHA-hsiRNA^{NTC}
ASO^{HTT}	Hung and Leeds, 2007; Exiqon	ASO-3209 (IONIS)
ASO^{NTC}	Exiqon	ASO-ContA
Oligonucleotides	This paper	Table S2
Software and Algorithms		
ImageJ	NIH	https://imagej.nih.gov/ij/
GraphPad Prism	GraphPad Software Inc.	https://www.graphpad.com/scientific-software/prism/
R	The R Foundation	https://www.r-project.org/
Other		
RNaseq	Blair et al., 2017	N/A
RNaseq	Zhang et al., 2014	https://web.stanford.edu/group/barres_lab/brain_rnaseq.html

CONTACT FOR REAGENT AND RESOURCE SHARING

Further information and requests for resources and reagents should be directed to and will be fulfilled by the Lead Contact, Anastasia Khvorova (Anastasia.khvorova@umassmed.edu).

EXPERIMENTAL MODEL AND SUBJECT DETAILS

Mice and Ethic Statements

Female wild-type FVB/NJ mice were purchased from The Jackson Laboratory and maintained in a specific pathogen-free facility. All procedures were performed in accordance with the National Institutes of Health Guideline for Laboratory Animals (including the timed pregnant mice used to obtain primary neurons) and were approved by the University of Massachusetts Medical School IACUC (Protocol #A2411).

Human Primary Cells

Adult dermal fibroblasts from healthy control were acquired from the Coriell Institute for Medical Research. Therefore, in regard to deidentified skin fibroblasts samples, we do not have access to the master list to reidentify subjects. This activity is not considered to meet federal definitions under the jurisdiction of an institutional review board and is thus exempt from the definition of human subject.

METHOD DETAILS

Cell Culture

HeLa and Neuroblastoma 2a (Neuro2a) cells were maintained in Dulbecco's Modified Eagle's Medium (DMEM) (Cellgro #10-013CV) supplemented with 10% fetal bovine serum (FBS; GIBCO #26140) and 100 U/ml Penicillin/Streptomycin (Invitrogen #15140) and grown at 37°C and 5% CO_2. Cells were split every 3-4 days.

The mouse primary fibroblasts were obtained from mouse dermal tissue following a method published by (Seluanov et al., 2010). Mouse and human primary fibroblast were maintained in MEM (GIBCO #11095) supplemented with 15% fetal bovine serum, 2% EAA (GIBCO #11130), 2% NEAA (GIBCO #11140), 1% vitamins (GIBCO #11120), 100 U/ml Penicillin/Streptomycin and pH7.4 and grown at 37°C and 5% CO_2. Cells were split every 3-4 days.

For FISH, cells were plated at 2.5×10^5 cells per dish on 35 mm glass bottom dishes (MatTek #P35G-1.5-10-C) pre-coated for one hour with poly-L-lysine (Sigma #P4707). Unless stated otherwise, the FISH procedure was performed at 2 days post-plating.

Conversion of Fibroblasts into Neuron-like Cells

The trans-differentiation of human primary fibroblasts into fibroblast-derived neurons was performed following the detailed protocol developed by (Richner et al., 2015). Briefly, the lentiviral cocktail of rtTA, pTight-9-124-BclxL, CTIP2, MYT1L, DLX1 and DLX2 was added to fibroblasts for 16 h, then cells were washed in PBS and cultured in fibroblasts medium (FM) containing 1 μg/mL doxycycline (DOX). At post-induction day (PID) 3, cells were cultured in FM containing 3 μg/mL puromycin, 3 μg/mL blasticidin and DOX. At PID 5 cells were replated onto sterile 24-wells glass-bottom plates (MatTek #P24G-1.5-10-F) pre-coated with polyornithine, fibronectin and laminin and cultured in FM + DOX. On PID 6, FM was replaced by Reprogramming Neuronal Medium (RNM): NbActiv4 (Brainbits #Nb4-500) with 200 μM dibutyl cyclic AMP, 1 mM valproic acid, 10 ng/mL BDNF, 10 ng/mL NT-3 and 1 μM retinoic acid, supplemented with DOX. Half-volume medium changes with RNM were performed every 4 days with addition of DOX every 2 days thereafter until PID 30–35. Addition of puromycin and blasticidin was terminated after PID 14.

Preparation of Primary Neurons

Primary cortical neurons were prepared and maintained as described in (Alterman et al., 2017). The procedure was performed using sterile standard dissection tools.

Primary cortical neurons were isolated from E16-17 mouse embryos of wild-type FVB/NJ mice. Pregnant females were anesthetized by intraperitoneal injection of Avertin at 250 mg per kg body weight (Sigma, #T48402) followed by cervical dislocation. Embryos were removed and transferred to ice-cold DMEM/F12 medium (Invitrogen #11320). Brains were removed and meninges were carefully detached. Cortices were isolated and transferred into pre-warmed papain solution for 25 min at 37°C, 5% CO_2 to dissolve the tissue. Papain (Worthington #54N15251) was dissolved in 2 mL Hibernate E (Brainbits #HE) and 1 mL EBSS (Worthington #LK003188), and supplemented with 0.25 mL of 10 mg/ml DNase1 (Worthington #54M15168) in Hibernate E. After the 25-30 min incubation, the papain solution was gently removed and 1 mL NbActiv4 (Brainbits #Nb4-500) supplemented with 2.5% FBS was added to the tissue. Tissues were then dissociated by gentle trituration through a fire-polished, glass Pasteur pipet. Neurons were counted, diluted at 1×10^6 cells/ml and plated as required for each experiment as described below. After overnight incubation at 37°C, 5% CO_2, an equal volume of NbActiv4 supplemented with anti-mitotics, 2.4 μg/ml 5-Fluoro-2'-deoxyuridine monophosphate (Sigma #F3503) and 4.8 μg/ml Uridine triphosphate (Sigma #U6625) to prevent the growth of non-neuronal cells, was added to neuronal cultures. Half of the volume of media was replaced with fresh NbActiv4 containing anti-mitotics every 48 hours until the experiments were performed.

FISH experiments

2×10^5 cells were plated in the glass center of 35 mm glass-bottom dishes (MatTek #P35G-1.5-10-C) pre-coated with poly-L-lysine (Sigma #P4707). Cells were fixed and processed for FISH five days post-preparation.

In vitro *silencing and cell viability assays*

1×10^5 neurons per well were plated on 96-well plates pre-coated with poly-L-lysine (BD BIOCOAT #356515) as described in (Alterman et al., 2017). Cells were processed 7 days post-treatment.

RT-qPCR

Experiments were performed with 2×10^6 cortical primary neurons plated on 6 cm plates, pre-coated with poly-D-lysine.

Oligonucleotides

Sequences and chemical modification patterns of siRNA^{HTT} and ASO^{HTT} are described in Table S2. All siRNAs design, synthesis and quality control have been performed in house and are available upon request. ASOs, designed by IONIS Pharmaceuticals (Hung and Leeds, 2007), have been purchased from Exiqon.

RNA Polymerase II Inhibition

Triptolide was dissolved in DMSO to a 10 mM stock concentration. Primary cortical neurons were treated with a final concentration of 25 μM triptolide (MedChemExpress #HY-32735) for indicated amount of time. Cells were fixed directly after treatment and processed for FISH experiment.

Cell Viability Assay

The oligonucleotide cytotoxicity was assessed *in vitro* in primary neurons in 96-well plates using alamarBlue reagent (Life Technologies #DAL1025) as recommended by manufacturer instruction. Briefly, 20 μl of alamarBlue reagent were added in 200 μl primary neurons culture medium and incubated for 4 hours. Resofurin fluorescence was measured at 550 nm excitation and 600 nm emission wavelengths.

Animal Stereotaxic Injections of Oligonucleotides

All mice used were wild-type female adults FVB/NJ, 14 weeks old at the time of the injection (The Jackson Laboratory). Prior to injection, mice were deeply anesthetized with 1.2% Avertin (Sigma #T48402). 4 nmol DHA-siRNA^{NTC}, DHA-siRNA^{HTT}, ASO^{NTC} or ASO^{HTT} (n = 3 mice per treatment group), diluted at 2 nmol/μl in aCSF, were administered by direct bollus microinjection into the right striatum by stereotaxic placement; coordinates (relative to bregma) were +1.0 mm anterio-posterior, +2.0 mm medio-lateral, and +3.0 mm dorso-ventral. All injection surgeries were performed using sterile surgical techniques and were accomplished using standard rodent stereotaxic instrument and an automated microinjection syringe pump (Digital Mouse Stereotaxic Frame; World Precision Instrument #504926). Mice were euthanized 7 days post-injection and brains were harvested.

Preparation of Mouse Brain Sections

Mice were sacrificed according to our institutional IAUCUC protocol (#A2411). Brains were removed, placed with eye bulbs facing upward in disposable cryomold (Polysciences, inc #18986-1), and frozen in O.C.T. embedding medium (Tissue-Tek #4583) in a dry ice/methanol bath. Brains were stored in −80°C and transferred at −20°C 24 hours prior sectioning. Brains were sliced into 20 μm brain sections using a cryostat (temperatures: sample holder −13°C, blade −12°C) (ThermoFisher CryoStar NX70) and mounted on superfrost slides (Fisher #1255015). Slides were stored at −80°C until further experiment.

Fluorescent *In Situ* Hybridization

FISH allows to perform single-cell detection of transcripts *in situ* and accurately quantify and report the relative levels of mRNA expression. Therefore, we compared the expression level of *Htt* mRNA with the expression level of housekeeping genes rather than normalize *Htt* mRNA level with any other control gene. mRNAs vary in sequence and length which may affect their subcellular localization. Thus, we investigated the cellular distribution of *Htt* mRNA with multiple transcripts: *1)* the conventional housekeeping mRNAs *ActB*, *Ppib* and *Hprt*; *2)* *Herc2* mRNA, selected because it is a transcript longer than *Htt* mRNA; *3)* *Neat*1 and *Malat1* long non-coding RNAs (lncRNAs) exclusively localized in the nucleus. The comparison of *Htt* mRNA level with multiple genes provided a more accurate and unbiased analysis of *Htt* transcript subcellular localization. See "Key Resources Table" for the detailed list and description of the genes assessed in this study.

Sample preparation

Cultured adherent cells were prepared as described by the manufacturer protocol for cultured adherent cells. Briefly, cells were fixed in 10% formalin for 20-30 min at 4°C and washed three times in PBS. Cells were dehydrated by sequential incubation in 50%, 70% and 100% ethanol for 1 min and incubated at least overnight and up to 6 months in 100% ethanol at −20°C. The day of FISH experiment, cells were re-hydrated by sequential incubation in 70% and 50% ethanol for 1 min followed by incubation in PBS for 10 min. Cells were incubated for 10 min in protease solution (Pretreat III) at room temperature. Cells were washed twice in PBS and processed for FISH.

Brain sections obtained on a cryostat were prepared as described by the manufacturer protocol for fresh frozen tissue (ACDBio #320513). Briefly, sections were fixed in 10% formalin for 15-20 min at 4°C and washed three times in PBS. Sections were dehydrated by sequential incubation in 50%, 70% and 100% ethanol for 5 min at room temperature and air-dried for 5 min at room temperature.

During this time the hydrophobic barrier around the sections can be drawn. Sections were incubated for 20-30 min in protease solution (Pretreat IV) at room temperature. Sections were washed twice in PBS and processed for FISH.

FISH experiments

FISH were performed using the RNAscope Fluorescent Multiplex kit (ACDBio #320850) following the manufacturer instruction (ACDBio #320293). Prior any experiment, we ensured that the probes were prewarmed at 40°C and cooled to room temperature to dissolve any crystal formed in the probe solution during storage at 4°C. Following sample preparation, samples were incubated with the target probe in the HybEZ oven at 40°C for 3 hours. The signal was amplified by incubation with the pre-amp, amp and label probes for 30 min each at 40°C. Between each incubation, samples were incubated in wash buffer twice for 2 min at room temperature. Following signal amplification, sample nuclei were stained with Dapi solution for 1 min, mounted in ProLong Gold antifade medium (ThermoFisher #P36930) and dried at room temperature overnight.

FISH-IF

Detection of NeuN and GFAP by immuno-fluorescence (IF) were performed following FISH experiment. Briefly, FISH procedure was performed as previously described by the manufacturer protocol followed directly by IF. Brain sections were incubated for 1 hour in blocking solution (2% Normal goat serum, 0.01% Triton-X in PBS) at room temperature. Slides were washed 3 times for 5 min in PBS. Brain sections were incubated in primary antibodies diluted in PBS (chicken monoclonal anti-NeuN 1:1000, Millipore #MAB377B; chicken polyclonal anti-GFAP 1:1000, Sigma #AB5541) overnight at room temperature. Slides were washed 3 times for 5 min in PBS and incubated for 1 hour at room temperature in secondary antibodies diluted in PBS. Slides were washed 3 times for 5 min in PBS, mounted in ProLong Gold antifade medium and dried at room temperature overnight.

Confocal Imaging

Images were acquired with a CSU10B Spinning Disk Confocal System scan head (Solamere Technology Group) mounted on a TE-200E2 inverted microscope (Nikon) with a 100x Plan/APO oil-immersion objective and a Coolsnap HQ2 camera (Roper Technologies). Z stacks were acquired using Micro-Manager by imaging at 0.5 μm intervals throughout the samples (brain section or cells). Consistent laser settings were used for all imaging sessions: 350 nm laser, 100 ms; 488 nm laser, 300 ms; 543 nm laser, 300 ms; gain 500. Images were processed using ImageJ software.

Cell Fractionation, RNA Isolation and qRT-PCR

Fractionation

At DIV8, neurons were lysed with 200 μl ice cold hypotonic lysis buffer (20 mM Tris-HCl pH7.5; 15 mM NaCl; 10 mM EDTA; 0.5% NP-40; 0.1% Triton X-100). Lysate was scraped from the plate and centrifuged at 1,200 x g for 10 min at 4°C to pellet nuclei. Cytoplasmic fractions were flash frozen and nuclear pellets were washed 2X in ice cold hypotonic lysis buffer and then flash frozen.

RNA extraction

Nuclear and cytoplasmic lysates were incubated in hypotonic lysis buffer/10% SDS/200 μg/ml proteinase K (ThermoFisher #AM2548) for 1 hour at 42°C, followed by acid phenol chloroform extraction, chloroform extraction, and ethanol precipitation. RNA was treated with Turbo DNase (ThermoFisher #AM9720), followed by cleanup with RNA Clean and Concentrator Kit (Zymo Research #R1015). Due to residual DNA contamination, nuclear fractions were DNase treated twice.

RT-qPCR

2 μg of cytoplasmic RNA or 1 μg of nuclear RNA was reverse transcribed using random hexamer priming and Superscript IV Reverse Transcriptase (ThermoFisher #18090010). cDNA was purified using Ampure beads (Agencourt #A63880) and amplified using Type-it Fast SNP Probe PCR Kit (QIAGEN #206045) and TaqMan MGB probes (ThermoFisher #4316034). Primer sequences are: *Htt* Exon 5 F-TGGTGCTCCTCGAAGTTTGC, R-TCCTCCGGTCTTTTGCTTGT; *Herc2* F- AGCCTTCTGCATCCTTGGTC, R-CGGAAGTCAGCAA TGGTCCT; ActB F-CTGTCGAGTCGCGTCCACC, R-CGCAGCGATATCGTCATCCA.

Htt mRNA Silencing Quantification

Htt mRNA silencing was performed as described in (Alterman et al., 2017). mRNA levels were assessed using the QuantiGene 2.0 Assay (Affymetrix #QS0011) and *Htt* mRNA level was normalized to *Ppib* mRNA (housekeeping control). Cells were lysed in 250 μL diluted lysis mixture per well (Affymetrix #13228) supplemented with 0.167 μg/μl proteinase K (Affymetrix #QS0103) for 30 min at 55°C. Cell lysates were mixed thoroughly and 40 μL (~16,000 cells) each lysate was added to the capture plate along with 40 μL additional diluted lysis mixture without proteinase K. Probe sets were diluted as specified in the Affymetrix protocol. 20 μL of mouse *Htt* or *Ppib* probe sets (Affymetrix #SB-14150, #SB-10002) was added for a final volume of 100 μL per sample well. The samples were incubated overnight at 55°C. The next day, the signal was amplified according to the Affymetrix QuantiGene protocol by incubating the samples with each probe for 1 hour: pre-amp and amp probes at 55°C and label probes at 50°C. Between each incubation, samples were washed three times in wash buffer at room temperature using a plate washer (Biotek EL$_X$-405). Luminescence was detected on a Veritas Luminometer (Promega). The average of the three technical replicates represents the mRNA expression value per sample.

Western Blot

Western blots were performed as described in (Keeler et al., 2016). Briefly, 10ug of primary neuronal lysates were separated by SDS-PAGE using 3%–8% Tris acetate gels (Life Technologies #EA03785BOX), transferred to nitrocellulose, blocked in 5%

milk/TBS + 0.1% Tween 20, incubated in primary antibody overnight at 4°C then secondary antibody 1 hour at room temperature. Signal was detected using Super Signal West Pico Chemiluminescent kit (Pierce #34080) and a CCD imaging system (Alpha Inno-tech) or Hyperfilm ECL (GE Healthcare #28906839) and densitometry was determined using ImageJ software (NIH). Primary antibodies were rabbit polyclonal anti-HTT antibody Ab1 (Sapp et al., 2012) (1:2000 in blocking buffer) and mouse monoclonal anti-GAPDH antibody (1:2000 in blocking buffer; Sigma #MAB374). Secondary antibodies were peroxidase-labeled anti-rabbit IgG (1:2500 in blocking buffer, Jackson Immunoresearch #711035152) or anti-mouse IgG (1:5000 in blocking buffer, Jackson Immu-noresearch #715035150).

QUANTIFICATION AND STATISTICAL ANALYSIS

Transcripts Localization and Quantification
Nuclear versus cytoplasmic localization analysis of RNA foci was performed with ImageJ (v1.51n) using a macro designed in house (Lawrence J. Hayward). Briefly, the 3D ROI Manager of Thomas Boudier (Ollion et al., 2013) was used to define individual fluorescent foci as 3D objects and to quantitate the integrated intensity of voxels within each object. Hoechst images were used to segment the nuclear regions in 3D. Distinct foci were segmented in 3D using radial Gaussian local thresholding from background-subtracted and filtered images, and the raw intensities within each 3D object were then integrated to obtain the total fluorescence signal. Following mRNA foci quantification in *Htt* mRNA silencing experiments, *Htt* mRNA levels were normalized to *Herc2* mRNA *in vitro* and *Hprt* mRNA level *in vivo*.

Co-Localization Quantification
Co-localization analysis was performed in ImageJ v1.51n (Schneider et al., 2012). To detect RNA foci, image stacks were convolved using a difference of Gaussians (DOG) method by using the 2D Gaussian filter (sigma = 134 nm, an approximation of a near-diffraction limited spot) and subtracting the same image stack with a larger Gaussian filter (sigma = 268 nm). The processed images were then thresholded using the Triangle method (Zack et al., 1977) thereby generating a binary image for each channel. Foci were converted to objects using the 3D objects counter plugin (Bolte and Cordelières, 2006) and co-localization was determined by calculating the fraction of overlapping objects in different channels. Co-localization values are reported as the percent of objects that are co-localized with a given label. To distinguish nuclear versus cytoplasmic RNA, the DAPI channel was convolved with a Gaussian filter (sigma = 670 nm) and thresholded using the Otsu method (Otsu, 1979). RNA foci overlapping the processed DAPI channel were considered nuclear and non-overlapping foci were considered cytoplasmic. Additionally, non-specific co-localization was calculated by rotating one of the channels over both the X- and Y-axes and re-calculating the co-localization using the same method. This allowed us to determine that co-localization was genuine and not simply due to random signal.

RNA-seq Data Analysis
Analyses of RNA-seq data were performed using the R statistical software environment.

Processed nuclear and cytoplasmic RNA-seq datasets across neuronal differentiation from (Blair et al., 2017) were downloaded from the Gene Expression Omnibus (GSE100007) and TPM values for *Htt* mRNA (ENSG0000197386) were extracted for plotting.

Expression of *Htt* mRNA across neuronal cell types was assessed on an interactive web browser (http://web.stanford.edu/group/barres_lab/brain_rnaseq.html) with data from (Zhang et al., 2014).

Statistical Analysis
Data analyses were performed using GraphPad Prism 7 software (GraphPad Software Inc.). Statistical parameters including the exact value of n, dispersion and precision measures (mean ± SEM) and statistical significance, denoted by asterisks (*, $p < 0.05$; **, $p < 0.01$; ***, $p < 0.001$; ****, $p < 0.0001$) are reported in the figures and figure legends. Data were analyzed using unpaired two-tailed t test, unpaired one-way or two-way ANOVA test with Bonferroni test for multiple comparison as specified in the figure legends. Differences in all comparisons were considered significant at $p < 0.05$. Randomization and investigator blinding were not considerations for this study design.